Journal of Radioanalytical and Nuclear Chemistry (2022) 331:889–902
https://doi.org/10.1007/s10967-021-08161-5

Introduction of phosphate groups into metal-organic frameworks to synthesize MIL-101(Cr)-PMIDA for selective adsorption of U(VI)

Xibiao Fu[1] · Jun Liu[2] · Zheng Ren[2] · Siqin Zhang[2] · Fangzhu Xiao[3] · Guowen Peng[1,2,4]

Received: 17 September 2021 / Accepted: 10 December 2021 / Published online: 25 January 2022

Abstract

Metal-organic frameworks (MOFs) MIL-101(Cr)-PMIDA with phosphate groups were prepared for the adsorption of U(VI). The morphology and structure of the samples were characterized by SEM, TEM, FT-IR, BET, XPS and XRD. This study investigated the effects of the initial U(VI) concentration, contact time, pH, adsorption temperature and coexisting ions on the adsorption of U(VI) by MIL-101(Cr)-PMIDA. The experimental results showed that the adsorption capacity of MIL-101(Cr)-PMIDA was 267.92 mg g^{-1} at C_0 (U) = 40 mg L^{-1}, pH = 6.0 and T = 298 K, which was much higher than that of MIL-101(Cr)-NH_2 (71.10 mg g^{-1}). More importantly, the material exhibited excellent selective removal performance for U(VI) in an aqueous solution. Furthermore, adsorption thermodynamics and kinetic studies showed that the adsorption was spontaneous ($\Delta G < 0$) and exothermic (ΔH ˃ 0), following the pseudo-second-order kinetic model ($R^2 > 0.99$).

Graphical abstract

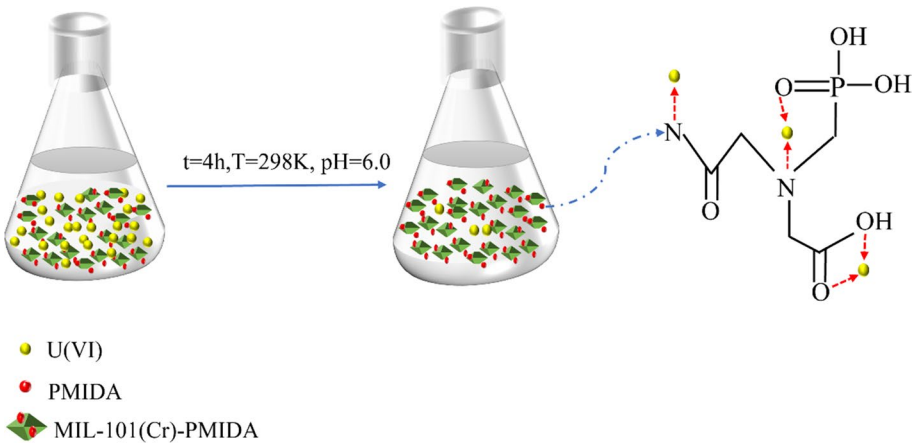

Keywords Metal-organic frameworks · Phosphate group · U(VI) · Adsorption

Xibiao Fu and Jun Liu have contributed equally to this work.

✉ Fangzhu Xiao
xfzhunh@163.com

✉ Guowen Peng
pgwnh78@163.com

[1] School of Chemistry and Chemical Engineering, University of South China, Hengyang 421001, Hunan, People's Republic of China

[2] School of Resources Environment and Safety Engineering, University of South China, Hengyang 421001, Hunan, People's Republic of China

[3] School of Public Health, University of South China, Hengyang 421001, Hunan, People's Republic of China

[4] Hunan Engineering Research Center for the Safety Control and Recycling of Radioactive Heavy Metal Pollutants, University of South China, Hengyang 421001, Hunan, People's Republic of China

Introduction

As an efficient and clean energy source, nuclear energy is considered an alternative to traditional energy sources [1, 2]. However, the use of atomic energy inevitably releases large amounts of radioactive wastewater into the environment [3, 4]. Uranium is one of the main elements in radioactive wastewater [5]. At the same time, uranium is also a heavy metal ion that is toxic, mutagenic and carcinogenic, which causes catastrophic damage to aquatic biodiversity, thereby posing a further threat to human health [6–10]. In addition, uranium is a non-renewable resource [11]. From the perspective of sustainable resource utilization and environmental protection, the separation and recovery of uranium are of great importance [12]. In the past decades, the methods commonly used to separate uranium are ion exchange [13], chemical deposition [14], solvent extraction [15] and solid adsorption [16]. Compared with other separation technologies, the adsorption method has many advantages such as lower technical cost, more environmentally friendliness, and easier regeneration [17–19]. Currently, materials that have been widely used for the separation and removal of uranium include carbon-based materials [20], clay materials [21], metal–organic frameworks (MOFs) [22], organic polymers [23], etc. MOFs are often used to remove hazardous metal elements from aqueous solutions because of their high specific surface area, abundant binding sites and tunable pore size [24, 25].

MOFs are porous materials made of metal ions bridged with organic ligands and have excellent physicochemical properties widely used in gas storage, chemical catalysis, photoelectric sensing, and drug delivery [26–29]. Structurally and functionally tunable MOFs were also used to separate and remove U(VI) from uranium-containing wastewater and showed good removal capacity [30–33]. MIL-101(Cr) MOFs have been shown to exhibit excellent stability in acidic or basic solutions [34]. At the same time, MIL-101(Cr) has sufficiently large pores, which provide free access and a platform for metal ions to attach [35]. Although MIL-101(Cr) has excellent properties, it has limited active functional groups on its organic ligands, which limits its ability to remove U(VI) [36, 37]. Therefore, it is necessary to introduce some groups with coordination ability to U(VI) to change the surface affinity of the adsorbent to achieve efficient and selective adsorption of U(VI).

So far, most of the MOFs have been modified by introducing nitrogen-containing functional groups for U(VI) adsorption, such as MIL-101(Cr)-ED(ED = -$HNC_2H_4NH_2$) [36], MIL-101(Cr)-DETA(DETA = -$NHC_2H_4NHC_2H_4NH_2$)[35], MIL-101(Cr)-OA(OA = -CONHOH) [38], etc. It is well known that phosphate groups have high chemical stability and excellent affinity for U(VI) to maintain high adsorption capacity under acidic conditions [2, 39–41]. Lin et al. [42]. first synthesized UiO-68-P(O)$(OH)_2$ for uranium extraction from seawater and confirmed that P = O could form coordination group sequences with U(VI). Decker et al. [43]. found that CMPO@MIL-101 exhibited excellent selectivity for U(VI) in the presence of coexisting ions. It was shown that the targeted and selective extraction of U(VI) with MOFs modified with phosphate groups under acidic conditions was feasible.

In this paper, the adsorbent MIL-101(Cr)-PMIDA was prepared using the affinity of phosphate groups for U(VI). The effect of various parameters on the adsorption performance was investigated by batch experiments and the optimum adsorption conditions were determined. The adsorption mechanism was analyzed in detail by FT-IR and XPS spectroscopy. Finally, we determined the selective adsorption properties of MIL-101(Cr)-PMIDA on U(VI) under the interference of coexisting ions. This work promises to expand the application of MIL-101(Cr) porous materials in the field of uranium-containing wastewater.

Experimental

Materials

Uranyl nitrate hexahydrate ($UO_2(NO_3)_26H_2O$) were purchased from Shanghai Maclean Biochemicals Technology Co., Ltd. Chromium(III) nitrate ($Cr(NO_3)_39H_2O$, 99%), 2-aminoterephthalic acid(H_2BDC-NH_2, 99%), N-(phosphonomethyl) iminodiacetic acid (PMIDA, 95%), N, N'-dicyclohexylcarbodiimide (DCC, 99%), toluene(C_7H_8, 99%), methanol (CH_3OH, 99%), ethanol(C_2H_5OH, 99%) and N,N-dimethylformamide(DMF, 98%) were purchased from Aladdin Reagent (Shanghai, China) and used without further purification. Deionized water is prepared in the laboratory.

Preparation of adsorbents

Preparation of MIL-101(Cr)-NH_2

Preparation of MIL-101(Cr)-NH_2 was done according to the previous preparation method [44]. H_2BDC-NH_2 (0.54 g), Cr$(NO_3)_3$ $9H_2O$ (1.20 g), and NaOH (0.24 g) were dissolved in deionized water (30 mL), and the mixture was transferred to a steel autoclave lined with Teflon after ultrasonic dispersion and reacted in an oven at 423 K for 24 h. After cooling to room temperature, wash with ethanol and deionized water. The obtained green sample was transferred to the three-necked flask with a magnetic stirrer and refluxed with anhydrous ethanol for 12 h to remove unreacted H_2BDC-NH_2. Finally, the sample was dried in a vacuum drying oven at 373 K for 12 h.

Scheme 1 Synthesis procedure for MIL-101(Cr)-PMIDA

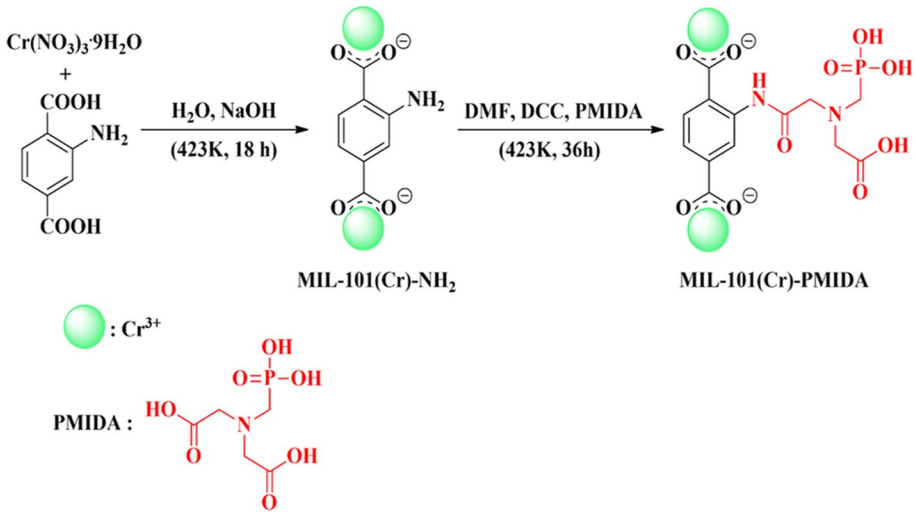

Preparation of MIL-101(Cr)-PMIDA

The MIL-101(Cr)-PMIDA was prepared according to literature with little modifications [45]. MIL-101(Cr)-NH_2 (0.50 g) and PMIDA (0.20 g) were added to DMF (85 mL) with ultrasonic stirring for 15 min, followed by the addition of DCC (0.30 g) to transfer the mixture to a round-bottom flask with a magnetic stirrer to warm up to 423 K for 36 h at reflux. After cooling to room temperature, the light green emulsion solid was collected by centrifugation, washed with toluene (2 × 30 mL) and methanol (2 × 30 mL), and dried under vacuum at 373 K for 8 h. (Scheme 1 Synthetic route of MIL-101(Cr)-PMIDA).

Characterization techniques

The U(VI) concentration in the solution was measured using a UV–Vis spectrophotometer (UV-2600, Shimadzu Corporation, Japan). The crystal structure of the sample was tested by XRD (Bruker D8 type, Bruker, Germany), Cu target, Kα radiation, Ni sheet filter, scan range $2\theta = 5°–90°$. The microstructure of the samples was observed using SEM (Zeiss Supra 40 type) and TEM (Talos F200X type). The specific surface area and pore volume of samples were determined at 423 K degassed at 77 K using a physisorption instrument (Micro for TriStar II Plus Model 2.02, Micro, USA). The adsorption mechanism was investigated using XPS (Esca lab model 250xi, Thermo Fisher Scientific, USA). The functional group peaks of the samples were analyzed by FT-IR (Nicolet-460, Thermo Fisher, USA) spectroscopy. The samples were analyzed qualitatively for elemental content using EDS (X-Max type, Oxford, UK).

Adsorption experiments

All adsorption experiments were performed by a batch method, and the pH of the solution was adjusted using 0.10 mol L^{-1} HNO_3 or 0.10 mol L^{-1} NaOH. In this experiment, 5.0 mg of adsorbent was dispersed into a 40 mL conical flask containing U(VI) solution, transferred to a constant temperature shaker for the adsorption reaction, and the supernatant was filtered using a 0.22 µm nylon membrane. For the detection of U(VI), filtered uranium solution (1.0 mL), and arsenazo III solution (1.0 mL) were added to the test tube. Next, dilute to 10.0 mL with acetic acid-sodium acetate buffer solution. Finally, the concentration of U(VI) in the solution was determined using a UV–Vis spectrophotometer at 652–655 nm. The desorption experiment was performed by dispersing 0.20 g of used adsorbent in HNO_3 solution for 12 h. After desorption, the samples were washed with HNO_3 solution and deionized water, and dried under vacuum at 373 K for 12 h. The adsorption capacity of the regenerated MIL-101(Cr)-PMIDA was measured by the above adsorption experiment method. The adsorption capacity q_e (mg g^{-1}), the adsorption rate R (%) was defined as in Eqs. (1–2)

$$q_e = \frac{(C_0 - C_e) \times V}{m} \quad (1)$$

$$R = \frac{(C_0 - C_e)}{C_0} \times 100\% \quad (2)$$

where C_0 and C_e are the initial (mg L^{-1}) and equilibrium concentrations (mg L^{-1}), respectively, V is the volume of the testing solution (mL), q_e is defined as the amount of adsorption and m corresponds to the mass of the adsorbent (mg). All experimental values were measured three times with errors within 5%.

Results and discussion

Structural, morphological and textural characterization

FT-IR analysis

Figure 1 shows the FT-IR spectra of MIL-101(Cr)-NH_2, MIL-101(Cr)-PMIDA and MIL-101-PMIDA (U). For MIL-101(Cr)-NH_2, the absorption bands of 3350–3510 cm^{-1} belonging to symmetric and asymmetric stretching vibrational peaks of N–H, which indicates the presence of amino groups [46]. 2920 cm^{-1}, 2980 cm^{-1} are attributed to C-H (aliphatic) stretching modes [47]. The peaks located at 1619 cm^{-1}, 598 cm^{-1} are attributed to the stretching vibration peaks of C = O, Cr–O, respectively [48]. 1260 cm^{-1}, 1387 cm^{-1}, reflected on the stretching vibrations of the C-N bonds and its splitting peaks, which confirmed the successful synthesis of MIL-101(Cr)-NH_2 [46]. For MIL-101(Cr)-PMIDA, two new characteristic peaks appeared at 1080 cm^{-1} and 918 cm^{-1} corresponding to P = O, P-OH stretching vibration peaks respectively, which tentatively indicated the successful modification of MIL-101(Cr)-NH_2 [49]. For MIL-101(Cr)-PMIDA(U), a new peak appears at 833 cm^{-1}, which is a characteristic symmetric absorption peak is ascribed to $[O=U=O]^{2+}$ [50]. Moreover, the characteristic peak of P = O changed in the adsorption U(VI), which indicates that P = O plays an active role in the adsorption process.

XRD analysis

XRD further analyzed MIL-101(Cr)-NH_2 and MIL-101(Cr)-PMIDA. As shown in Fig. 1b, the distinguishable diffraction peaks of MIL-101(Cr)-NH_2 appear at $2\theta = 5.50°$, 9.10°, 10.25° and 16.60°, corresponding to crystal planes (311), (753), (666) and (4416), respectively[51, 52]. The XRD diffraction peaks of MIL-101(Cr)-PMIDA and MIL-101(Cr)-NH_2 are surprisingly consistent, which indicates that the introduction of phosphate groups did not change the crystal structure of the raw material. Moreover, the XRD pattern of MIL-101(Cr)-PMIDA is consistent with the reported literature[53], which further illustrates the successful synthesis of the adsorbent.

BET analysis

The specific surface area and pore volume of MIL-101(Cr)-NH_2 and its phosphate derivatives were determined using N_2 physisorption measurements. As shown in Fig. 2a, MIL-101(Cr)-NH_2 and MIL-101(Cr)-PMIDA belong to the reversible type I isotherm, typical of porous materials [54]. The specific surface area and pore volume of MIL-101(Cr)-NH_2 were 1636.54 $m^2\ g^{-1}$ and 1.38 $cm^3\ g^{-1}$, which decreased to 1099.33 $m^2\ g^{-1}$ and 0.92 $cm^3\ g^{-1}$ after functionalization with phosphate groups, respectively. Combined with the FT-IR analysis, this is the grafted group occupying the material's pores, resulting in the reduction of the material's specific surface area and pore volume. As shown in Fig. 2b, the pore size distributions of MIL-101(Cr)-NH_2 and MIL-101(Cr)-PMIDA ranged from 3.16 to 4.52 nm and 3.16 to 4.39 nm, respectively. The pore size of the adsorbent is larger than the ion diameter, which is sufficient to allow the entry of uranyl ions [45].

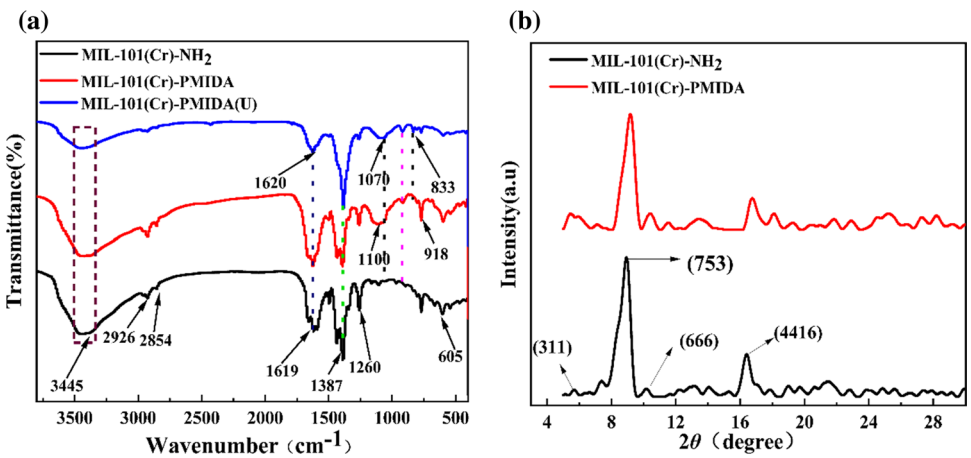

Fig. 1 FT-IR spectra of MIL-101(Cr)-NH_2, MIL-101(Cr)-PMIDA and MIL-101(Cr)-PMIDA (U) (**a**), XRD patterns of MIL-101(Cr)-NH_2 and MIL-101(Cr)-PMIDA (**b**)

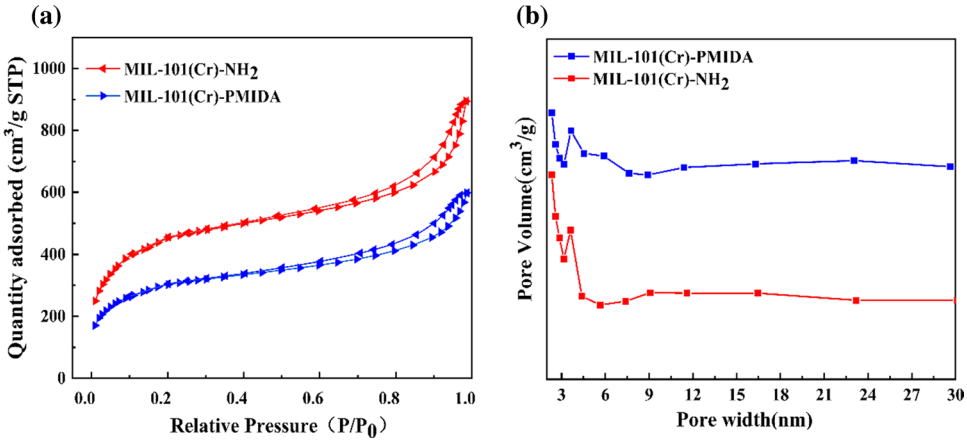

Fig. 2 N_2 adsorption/desorption isotherm of MIL-101(Cr)-NH_2 and MIL-101(Cr)-PMIDA (**a**), BJH pore size distribution of MIL-101(Cr)-NH_2 and MIL-101(Cr)-PMIDA(**b**)

SEM, TEM and EDS analysis

Figure 3 shows the TEM and SEM images of the MIL-101(Cr)-NH_2 and its phosphate derivatives. As can be seen from the Fig. 3(a, b, c), the morphology of the material did not change significantly after grafting the functional groups. As shown in Fig. 3(d, e, f), the crystal particles of MIL-101(Cr)-NH_2 and MIL-101(Cr)-PMIDA are homogeneous with a size of about 50 nm and a shape similar to that reported in the literature[55]. Moreover, comparing the TEM and SEM images of the two materials, no significant changes were observed, further indicating that the framework structure and morphology of the MOFs maintained some stability during functionalization. EDS qualitatively analyzed the chemical composition of the MOFs, and the presence of P, N, O, C, and Cr elements is seen in Fig. 4a, after the adsorption (Fig. 4b) appears with U(VI) elemental content. The combination of EDS, XPS, FT-IR and XRD finally confirmed the synthesis of MIL-101(Cr)-PMIDA and the adsorption of U(VI).

Effect of pH

U(VI) exists in different forms at different pH conditions, so pH is an important parameter affecting the separation of U(VI)[36]. As shown in Fig. 5, when pH < 6.0, U(VI) usually exists in the form of uranyl ion (UO_2^{2+}) in the aqueous solution, U(VI) will hydrolyze to form polynuclear hydroxide at pH > 6.0[56]. Therefore, in this experiment, pH values of 2.0 to 6.0 were chosen to investigate the effect of different pH values on the adsorption of U(VI) by MIL-101(Cr)-PMIDA. The experimental results showed that the adsorption capacity of both adsorbents depended on the pH of the solution (as shown in Fig. 6). At pH < 4.0, the phosphate groups protonation weakened the adsorbent's binding ability to the target ions, which limited the adsorption capacity of MIL-101(Cr)-PMIDA [57]. With the increasing pH value, the functional groups of adsorbent deprotonated and the electrostatic repulsion weakened, which led to a rapid enhancement in adsorption capacity [58]. At pH = 6.0, the saturated adsorption capacity of MIL-101(Cr)-PMIDA was 267.92 mg g^{-1}, which was much higher than the adsorption capacity of MIL-101(Cr)-NH_2 (71.10 mg g^{-1}). MIL-101(Cr)-PMIDA maintains a high adsorption capacity, which may be attributed to the excellent affinity of the phosphate group for U(VI). To obtain a high adsorption capacity, pH 6.0 was chosen for subsequent adsorption experiments.

Effect of initial concentration

As shown in Fig. 7, the adsorption capacity of MIL-101(Cr)-PMIDA gradually increased with the initial U(VI) concentration, at C_0 (U) = 40 mg L^{-1}, the adsorption capacity and removal rate were 263.92 ± 7.10 mg g^{-1} and 82.5%, respectively. When the initial U(VI) concentration was greater than 40 mg L^{-1}, the rise of the adsorption capacity slowed down and the removal rate decreased sharply, finally reaching the adsorption equilibrium at the initial U(VI) concentration equal to 100 mg L^{-1} with an equilibrium adsorption capacity of 328.5 mg g^{-1}. This phenomenon suggests that the concentration difference drives the transfer of U(VI) from the aqueous solution to the surface of MIL-101(Cr)-PMIDA until the adsorption saturation of the active site of the adsorbent is reached. In Table 1, The MIL-101(Cr)-PMIDA showed an excellent adsorption capacity compared with other reported adsorbents. In order to obtain high adsorption capacity and adsorption rate, the initial U(VI) concentration of 40 mg L^{-1} was selected for experimental investigation in the subsequent experiments.

Adsorption kinetics

To explore the adsorption mechanism of U(VI) on MIL-101(Cr)-PMIDA, 5.0 mg of adsorbent was dispersed in C_0 = 40 mg L^{-1} of U(VI) solution with contact time (5–360 min). As shown in Fig. 8, the adsorption process

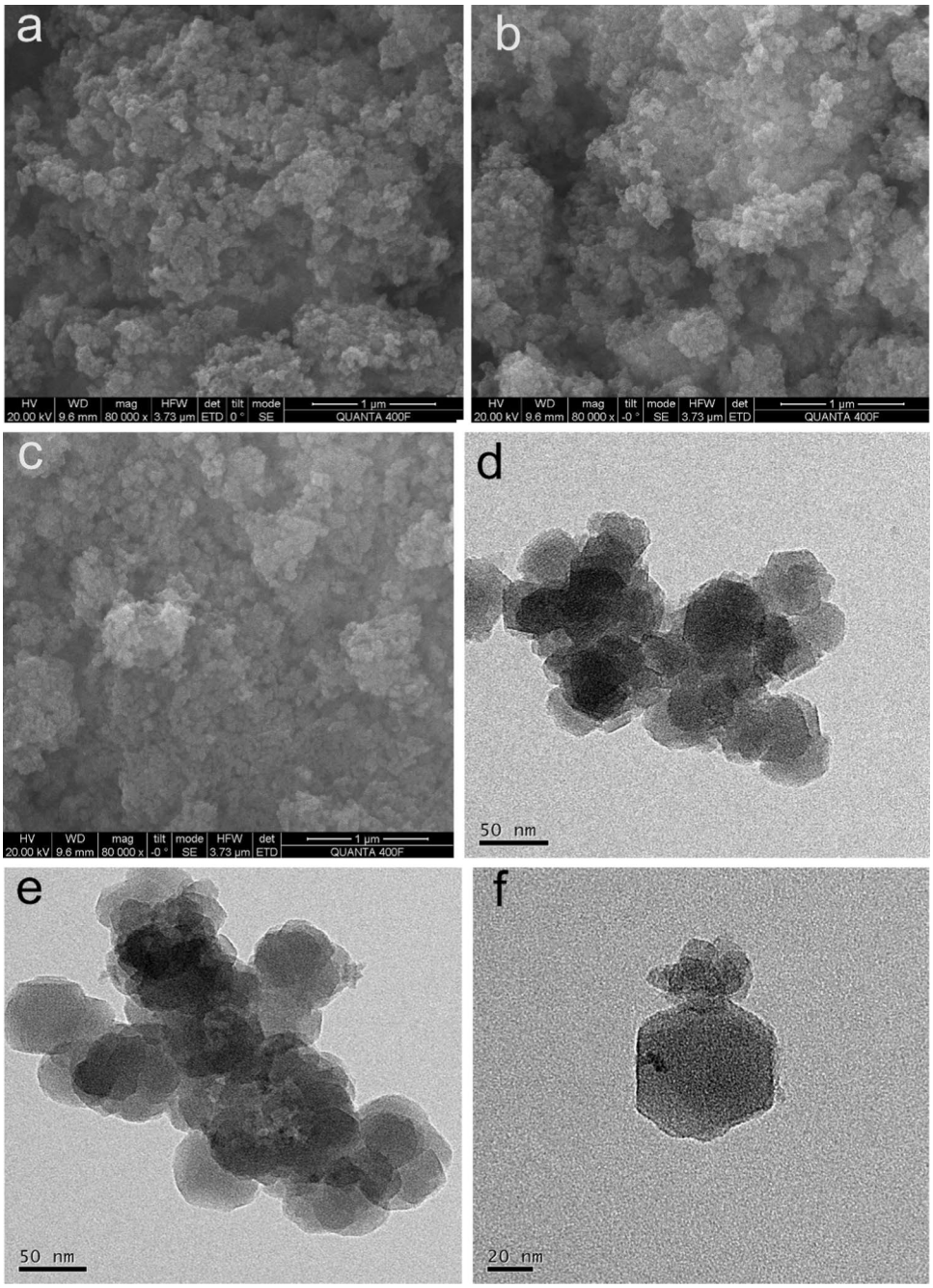

Fig. 3 SEM images of MIL-101(Cr)-NH_2 (**a**), MIL-101(Cr)-PMIDA (**b**, **c**), TEM images of MIL-101(Cr)-NH_2 (**d**), MIL-101(Cr)-PMIDA (**e**, **f**)

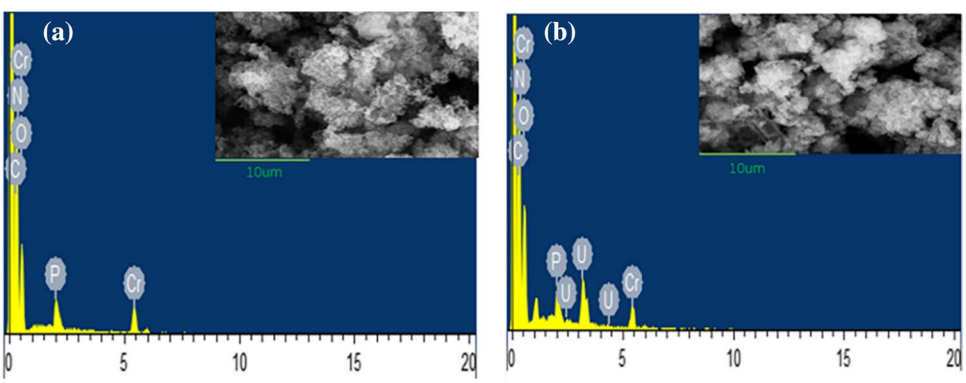

Fig. 4 EDS images of MIL-101(Cr)-PMIDA (**a**) and MIL-101(Cr)-PMIDA(U) (**b**)

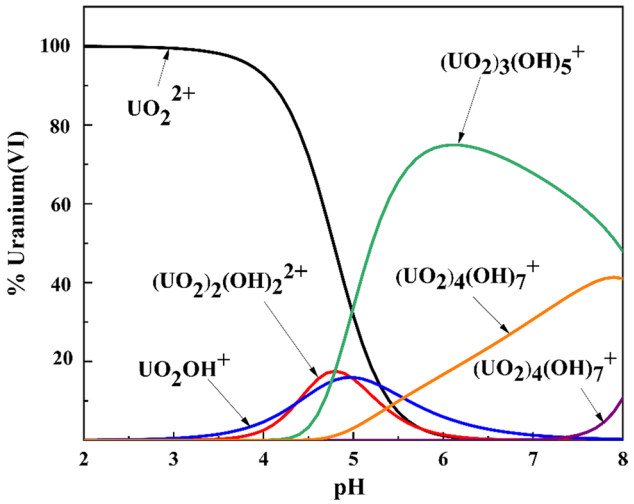

Fig. 5 Distribution of U(VI) species in aqueous solution obtained by Visual MINTEQ 3.1 simulation (pH = 2.0–8.0, C_0(U) = 40 mg L^{-1})

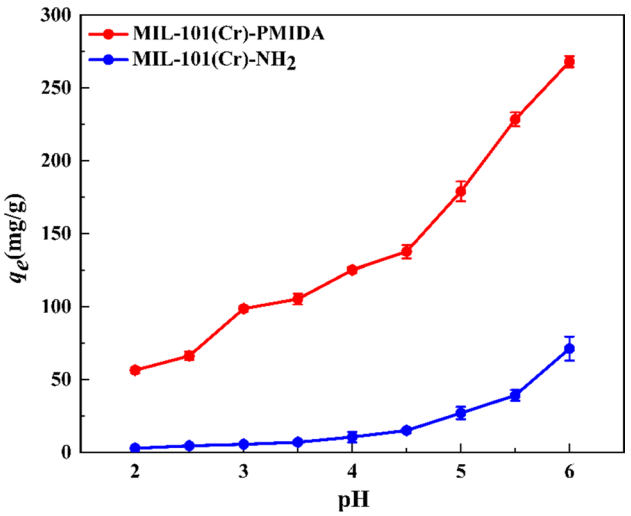

Fig. 6 Effect of pH on the U(VI) adsorption onto MIL-101(Cr)-NH_2 and MIL-101(Cr)-PMIDA (t = 240 min, m = 5.0 mg, V = 40 mL, C_0(U) = 40 mg L^{-1}, T = 298 K)

can be divided into three parts: (1) Within 90 min, the adsorbent surface and pore channels provided sufficient active sites, so the adsorption rate increased rapidly. (2) During 90–180 min, the active sites on the adsorbent surface were gradually occupied, and the U(VI) diffusion rate in the pore channels was limited, so the adsorption rate decreased. (3) The adsorption saturation was reached after 180 min, and the equilibrium adsorption amount $q_{e,\,exp} = 260.9 \pm 5.20$ mg g^{-1}. The pseudo-first-order kinetics and the pseudo-second-order kinetics were used to explore the adsorption process, the two models expressions are shown in Eqs. (3–4) [59].

The pseudo-first-order Eq:

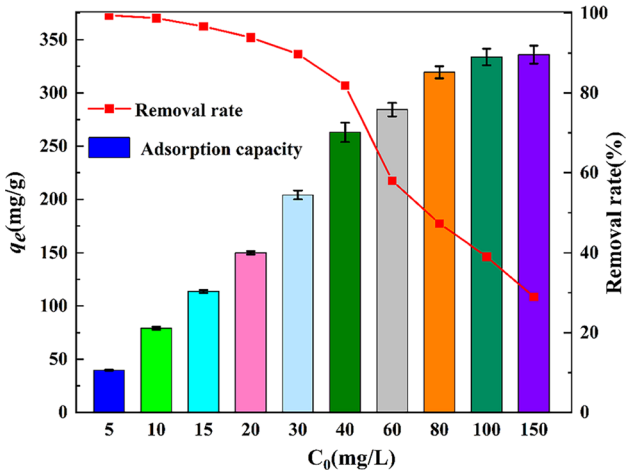

Fig. 7 The effect of U(VI) initial concentration on the adsorption capacity (m = 5.0 mg, V = 40 mL, t = 240 min, T = 298 K, pH = 6.0)

$$\ln\left(q_e - q_t\right) = \ln q_e - k_1 t \tag{3}$$

The pseudo-second-order Eq:

$$\frac{t}{q_t} = \frac{1}{k_2 q_e^2} + \frac{t}{q_e} \tag{4}$$

Here q_t (mg g^{-1}) and q_e (mg g^{-1}) is the adsorption capacity of the adsorbent at moment t and at equilibrium, respectively. k_1 (min^{-1}) and k_2 (g (mg min)$^{-1}$) are the rate constants for the two kinetic models, respectively.

As shown in Fig. 9(a, b), the linear correlation of the pseudo-second-order fit is significantly better than that of the pseudo-first-order kinetic model. The two kinetic parameters calculated from the slope and intercept of the straight line are shown in Table 2. The correlation coefficient of the pseudo-first-order kinetic model is $R^2 = 0.918$, and the correlation coefficient of the pseudo-second-order kinetic model is $R^2 = 0.998$. Meanwhile, the saturation adsorption amount $q_{e,\,cal} = 277.8$ mg g^{-1} obtained by the pseudo-second-order kinetic model is close to the experimentally tested equilibrium amount $q_{e,\,exp} = 260.90$ mg g^{-1}. The fitting results indicate that the pseudo-second-order kinetic model is more suitable to describe the adsorption process of U(VI) on MIL-101(Cr)-PMIDA, and the adsorption process is mainly the chemical adsorption [60].

Adsorption isotherms and thermodynamics

To analyze the adsorption mechanism of MIL-101(Cr)-PMIDA, the adsorption isotherms of U(VI) solutions with concentrations ranging from 10 to 100 mg L^{-1} at 288 K, 298 K and 308 K were investigated (as shown in **Fig. 10**). Langmuir and Freundlich isotherm models were used to fit

Table 1 Comparison of the capacity of MIL-101(Cr)-PMIDA with other absorbents

Adsorbents	Exp. Conditions	q_e (mg g^{-1})	References
MIL-53(Al)-AO	pH = 6.0, C_0 = 100 mg L^{-1}	100.0	[31]
UIO-66-AO	pH = 5.5, C_0 = 100 mg L^{-1}	195.0	[32]
MIL-101-OA	pH = 8.0, C_0 = 100 mg L^{-1}	321.0	[38]
MIL-101-ED	pH = 5.5, C_0 = 100 mg L^{-1}	200.0	[36]
MIL-101-DETA	pH = 5.5, C_0 = 100 mg L^{-1}	350.0	[35]
UiO-68-PO_4Et_2	pH = 2.5, C_0 = 100 mg L^{-1}	217.0	[42]
GO-COOH/UIO-66	pH = 8.0, C_0 = 100 mg L^{-1}	188.3	[64]
MIL-101(Cr)-PMIDA	pH = 6.0, C_0 = 100 mg L^{-1}	328.5	This work

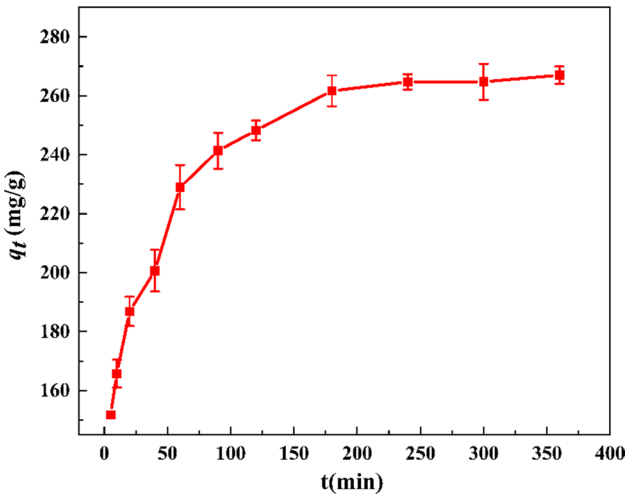

Fig. 8 Effect of contact time on the adsorption of U(VI) (m = 5.0 mg, V = 40 mL, T = 298 K, C_0(U) = 40 mg L^{-1}, pH = 6.0)

the adsorption process, and the two model-fitting equations are shown in Eq. (5–6)

$$\frac{C_e}{q_e} = \frac{1}{K_L q_m} + \frac{C_e}{q_m} \tag{5}$$

$$\ln q_e = \ln K_F + \frac{1}{n} \ln C_e \tag{6}$$

where C_e is the equilibrium U(VI) concentration (mg L^{-1}), q_m is the maximum adsorption capacity (mg g^{-1}), K_L is Langmuir isothermal constant, K_F and n are the Freundlich isothermal constants related to adsorption capacity and strength, respectively.

Based on the correlation parameters calculated from the linear fit (Fig. 11), as shown in Table 3, the correlation coefficients of the Langmuir isotherm model ($R^2 > 0.99$) are all greater than those of the Freundlich isotherm model. This indicates that U(VI) is uniformly adsorbed on the binding sites on the surface of MIL-101(Cr)-PMIDA, which is a monomolecular layer adsorption process[61].

Temperature affects the degree of ion diffusion and the affinity of active sites on the adsorbent surface, so we investigated the effect of temperature on the adsorption of U(VI) by MIL-101(Cr)-PMIDA. As shown in Fig. 12a, the adsorption capacity increased with increasing temperature over a specific temperature range. A plausible explanation is that the molecular motion becomes active with increasing temperature, which increases the possibility of contact of the adsorbent with U(VI)[62]. Calculating the thermodynamic parameters enthalpy change (ΔH^0),

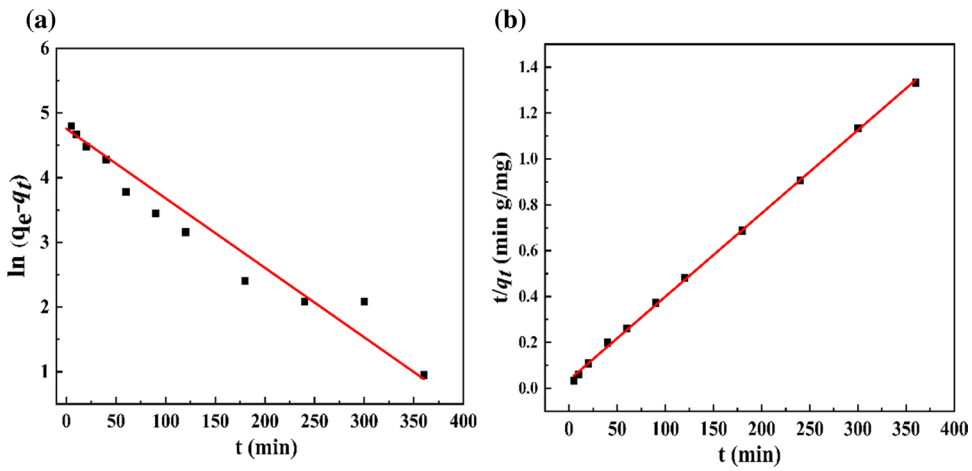

Fig. 9 Fitting results of two known kinetic models, **a** pseudo-first-order kinetic model and **b** pseudo-second-order kinetic model (C_0(U) = 40 mg L^{-1}, pH = 6.0, m = 5.0 mg, V = 40 mL, T = 298 K)

Table 2 Kinetic parameters of two models

Pseudo-first-order kinetic model			Pseudo-second-order kinetic model		
$q_{e,cal}$ (mg g^{-1})	k_1 (min^{-1})	R^2	$q_{e,cal}$ (mg g^{-1})	k_2 (g mg^{-1} min^{-1})	R^2
127.74	0.0107	0.918	277.78	0.0003536	0.999

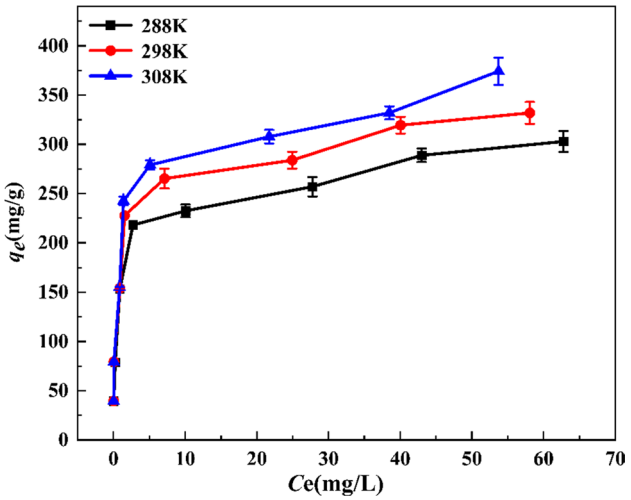

Fig. 10 Adsorption isotherms for U(VI) on MIL-101(Cr)-PMIDA at different temperatures (m = 5.0 mg, pH = 6.0, t = 240 min, V = 40 mL)

entropy change (ΔS^0), and Gibbs free energy (ΔG^0) helps to further understand the adsorption process. The thermodynamic parameters are calculated as in Eqs. (7–9) [63].

$$K_d = \frac{q_e}{C_e} \tag{7}$$

$$\ln K_d = -\frac{\Delta H^0}{RT} + \frac{\Delta S^0}{R} \tag{8}$$

$$\Delta G^0 = \Delta H^0 - T\Delta S^0 \tag{9}$$

where K_d is the distribution coefficient (mL g^{-1}), T is the adsorption temperature (K), R is the ideal gas constant (8.314 J mol^{-1} K^{-1}), ΔH^0 (kJ mol^{-1}) is the enthalpy change and ΔS^0 (J mol^{-1} K^{-1}) is the entropy change, the slope and intercept of the curve of $\ln K_d$ versus $1/T$ correspond to ΔH^0 and ΔS^0, respectively (as shown in Fig. 12b). As Table 4 records the thermodynamic calculations, negative values of ΔG^0 indicate that the adsorption process is spontaneous, and ΔG^0 decreases gradually with increasing temperature, indicating that increasing temperature is favorable for adsorption[64]. In addition, the positive values of ΔH^0 and ΔS^0 indicate that the adsorption is an endothermic entropy-increasing process.

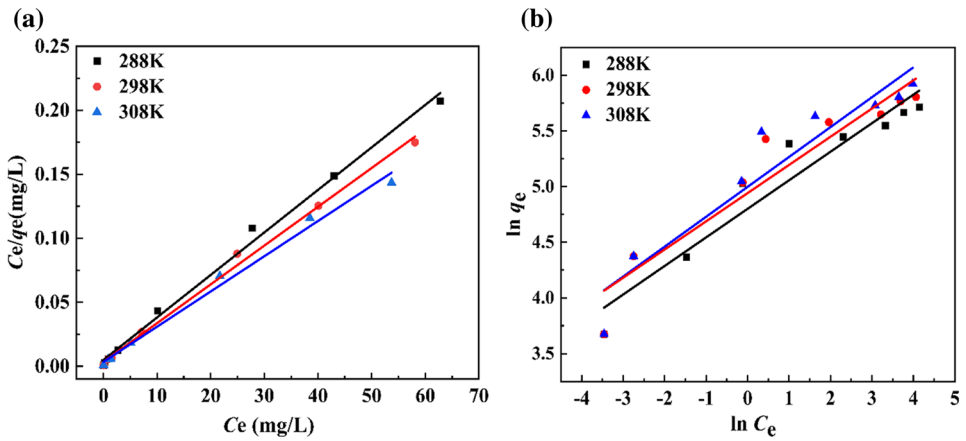

Fig. 11 Linear fitting results of Langmuir (**a**) and Freundlich (**b**) adsorption isotherms (m = 5.0 mg, t = 240 min, pH = 6.0, V = 40 mL)

Table 3 Parameters of two isotherm models

T (K)	Langmuir Isotherm			Freundlich Isotherm		
	q_m (mg g^{-1})	k_L (L mg^{-1})	R^2	k_F ((mg g^{-1}) $(L{\cdot}mg)^{1/n}$)	n	R^2
288 K	301.210	0.672	0.994	121.576	3.900	0.910
298 K	332.226	0.893	0.996	140.004	3.950	0.886
308 K	370.370	0.799	0.991	148.096	3.726	0.887

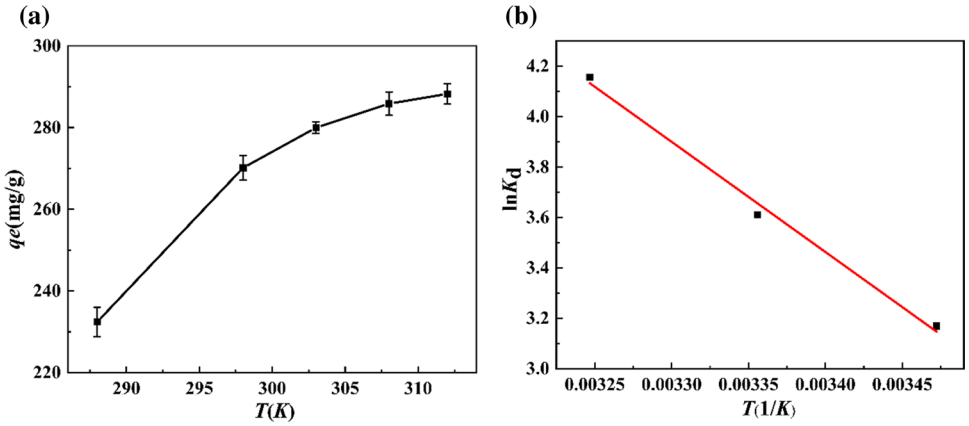

Fig. 12 Effect of temperature on adsorption capacity (**a**), the linear fitting curve of adsorption thermodynamics (**b**) (pH = 6.0, m = 5.0 mg, C_0 (U) = 40 mg L^{-1}, t = 240 min, V = 40 mL)

Table 4 Thermodynamic parameters of U(VI) adsorption on MIL-101(Cr)-PMIDA

T(K)	lnK_d	ΔH^0 (kJ mol^{-1})	ΔS^0 (J K^{-1} mol^{-1})	ΔG^0 (kJ mol^{-1})
288 K	3.169	38.251	160.631	− 8.034
298 K	3.611	38.251	160.631	− 9.641
308 K	4.156	38.251	160.631	− 11.248

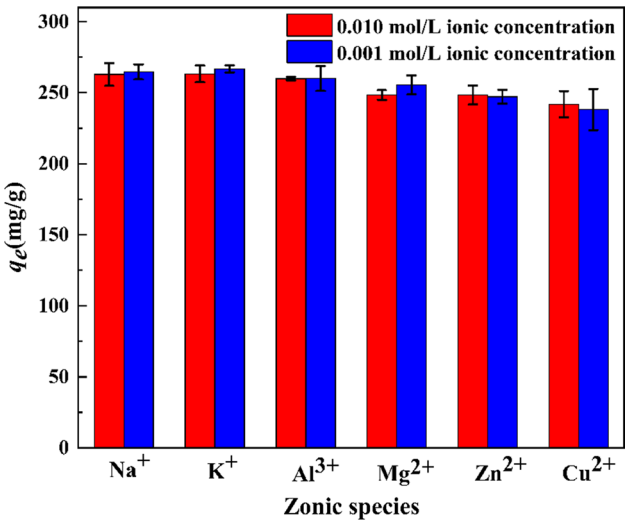

Fig. 13 Effect of interfering ions on the adsorption of U(VI) by MIL-101(Cr)-PMIDA (C_0(U) = 40.0 mg L^{-1}, m = 5.0 mg, pH = 6.0, t = 240 min, T = 298 K, V = 40 mL)

Selective adsorption of U(VI)

Considering that U(VI) and other metal ions usually coexist in radioactive wastewater, the practical application requires adsorbents with selective removal function for U(VI). Therefore, binary aqueous solutions containing U(VI) (40 mg L^{-1}) solution and coexisting cations (Na^+, k^+, Mg^{2+}, Zn^{2+}, Al^{3+}, Cu^{2+} = 0.001 mol L^{-1} and 0.010 mol L^{-1}) were prepared to investigate the effect of coexisting cations on the adsorption performance. As shown in Fig. 13, there was no significant inhibition of the adsorption capacity by the interfering ions. The adsorption amounts were all above 230 mg g^{-1}, which may be due to the affinity of the phosphate group for U(VI). The experiments have shown that MIL-101(Cr)-PMIDA has excellent selective adsorption capacity for U(VI) in solutions of coexisting cations and is a potential adsorbent for U(VI) separation from radioactive wastewater.

Desorption and reusability of the MIL-101(Cr)-PMIDA

As shown in Fig. 6, the adsorption capacity is weaker at pH < 3.0, which indicates that acid washing is one of the possible ways to regenerate desorption. To study the reusability of MIL-101(Cr)-PMIDA, 0.1, 0.2, 0.3, 0.5, 0.7 and 1.0 mol L^{-1} HNO_3 solutions were used as eluents to desorb the used adsorbents. As shown in Fig. 14a, the desorption capacity increases with the increase of HNO_3 concentration. When HNO_3 is 0.3 mol L^{-1}, the desorption capacity reaches saturation. In this reusability study, the used adsorbent was desorbed with 0.3 mol L^{-1} HNO_3 for 12 h, washed sequentially with 0.3 mol L^{-1} HNO_3 and deionized water, dried under vacuum at 373 K for 12 h, and then subjected to four adsorption–desorption cycles of adsorption experiments. Here, 5.0 mg of the adsorbent was added to 40 mL of U(VI) solution with a concentration of 40 mg L^{-1} to explore the reusability of the adsorbent. Figure 14b shows that the adsorption capacity decreases with the increasing number of desorptions during the adsorption/desorption cycle. After four consecutive adsorption/desorption cycles, the adsorption capacity was higher than 180 mg g^{-1}, proving that the material had good regeneration performance and reusability. The main reason for the decrease in adsorption capacity is the incomplete elution of MIL-101(Cr)-PMIDA material and the trace loss of adsorbent during the circulation process.

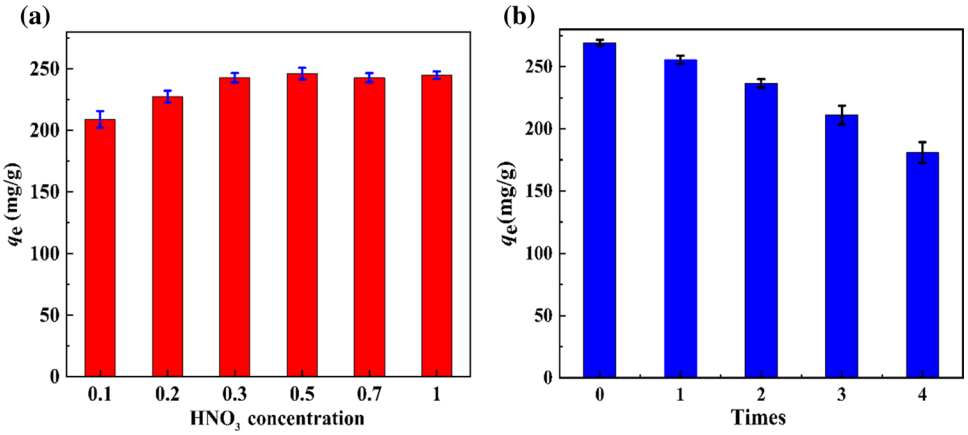

Fig. 14 Effect of different HNO_3 concentration on desorption (**a**), effect of number of cycles on the adsorption capacity (**b**)

XPS analysis and mechanism exploration

The adsorption mechanism of U(VI) on MIL-101(Cr)-PMIDA was analyzed by XPS high-resolution spectroscopy. As shown in Fig. 15b, U4f peaks appear at 382.25 eV and 392.86 eV, which are attributed to U $4f_{7/2}$ and U $4f_{5/2}$ respectively, and the spin–orbit split is 10.6 eV [65]. Similarly, the peaks of the p element appear at 133.10 eV and 191.10 eV, which belong to the high-resolution spectra of P2p and P2s, respectively [66].

As shown in Fig. 15d, the P2p high-resolution spectrum before adsorption could be divided into $P2p_{1/2}$ (132.83 eV) and $P2p_{3/2}$ (133.51 eV) for P-OH and P = O, respectively [67]. After adsorption, the P = O binding energy shifts to 133.83 eV (Fig. 15c), while the binding energy of P-OH changes less (133.88 eV). The shift of the P peak is because the O element bound to P provides a lone pair of electrons coordinated to U(VI), which leads to a shift in the P = O binding energy [68]. Combined with FT-IR analysis, the P = O bond is involved in the binding of U(VI).

As shown in Fig. 15f, O1s before adsorption can be divided into four peaks (530.59 eV, 531.27 eV, 531.97 eV and 532.68 eV) attributed to O-C = O, P = O, C = O, P-OH, respectively [69]. After adsorption (Fig. 15e), the binding energies of O-C = O and P = O shifted to 530.70 eV and 531.45 eV, indicating that the O-C = O and P = O bonds are involved in the U(VI) coordination. In contrast, the binding energies of C = O and P-O (532.04 eV, 532.73 eV) changed less and may not be involved in the U(VI) complexation reaction.

As shown in (Fig. 15h), for N1s the adsorption spectrum can be roughly divided into three peaks (399.36 eV, 400.36 eV and 401.31 eV) attributed to -NH-, R_3N- and R_3NH^+-, respectively [70, 71]. After adsorption (Fig. 15g) -NH-, R_3N- and R_3NH^+- binding energies are transferred to 399.57 eV, 400.52 eV and 401.44 eV, respectively. Based on the XPS analysis of the high-resolution spectra of P, N, and O elements, we inferred U(VI) binding mode to MIL-101(Cr)-PMIDA in an aqueous solution: (1) O-C = O and -NH- bonds are combined with U(VI) respectively. (2) The lone electron pair of the N element and the P = O bond form a complex coordination bond with U(VI).

Conclusions

In summary, the following conclusions could be drawn: (1) MIL-101(Cr)-PMIDA adsorbent with high adsorption capacity on U(VI) was synthesized by introducing PMIDA onto the amine group of MIL-101(Cr)-NH_2 using a simple and efficient post-modification synthesis technique. (2) XPS spectrum analysis showed that the functional groups (O-C = O, P = O, R_3N-, -NH-) on the surface of the adsorbent were involved in the binding of U(VI). (3) The thermodynamic calculation parameters showed that adsorption was a spontaneous entropy-increasing process and heating up was beneficial to adsorption. (4) The pseudo-second-order kinetic model was more suitable for describing the adsorption process, and the adsorption isotherms were consistent with the Langmuir isotherm model, reflecting that the adsorption of U(VI) by MIL-101(Cr)-PMIDA was dominated by chemisorption. (5) MIL-101(Cr)-PMIDA adsorbent showed excellent selectivity for U(VI) in competition adsorption with metal ions (Na^+, k^+, Mg^{2+}, Zn^{2+}, Al^{3+}, Cu^{2+}). (6) Using 0.3 mol L^{-1} HNO_3 as the desorption agent, the adsorption capacity was higher than 180 mg g^{-1} in all four consecutive adsorption/desorption cycles. Based on the present results, MIL-101(Cr)-PMIDA is an excellent performance adsorbent with good application prospects in the field of uranium-containing wastewater treatment.

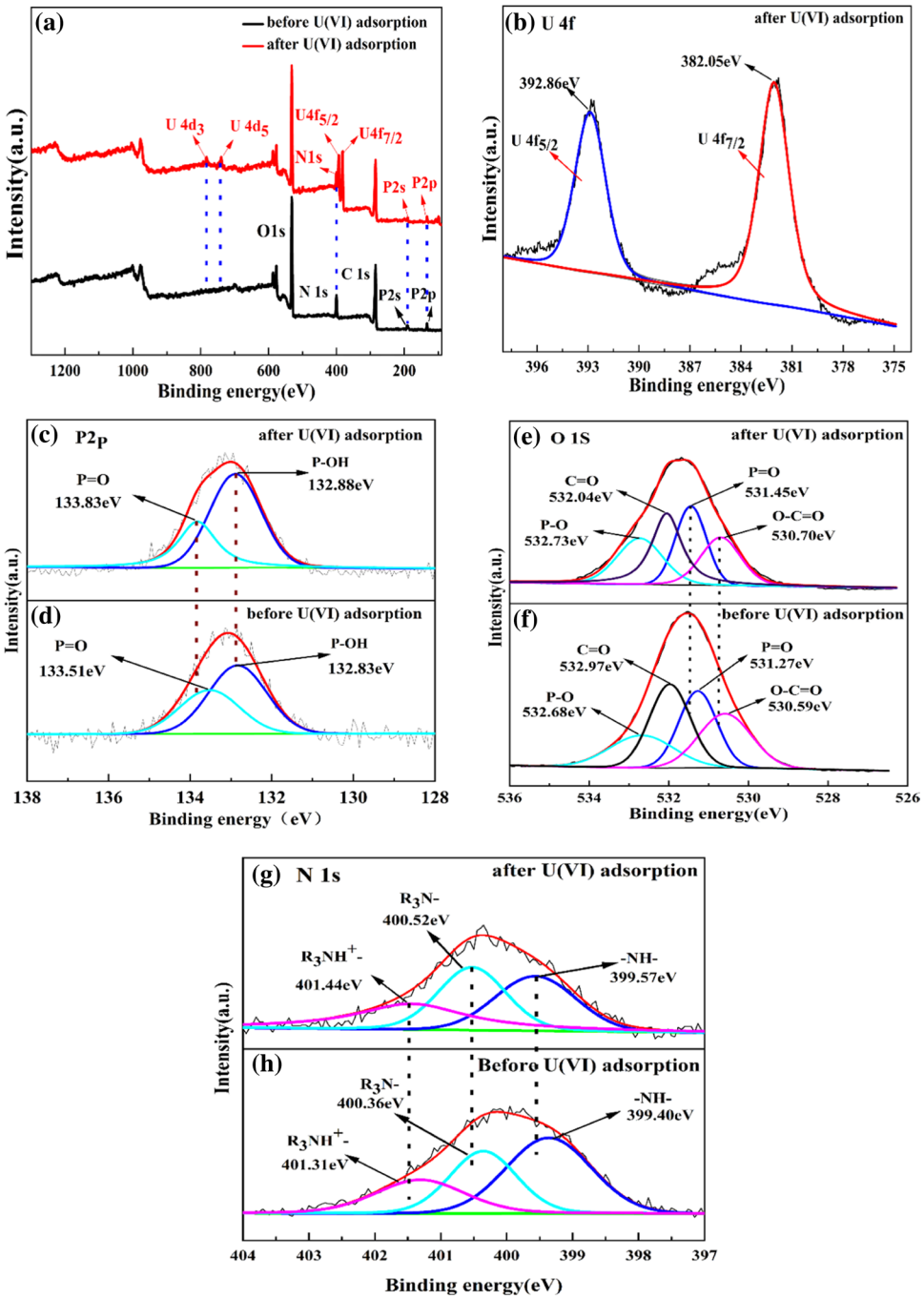

Fig. 15 Wide XPS survey (**a**), high-resolution U 4f (**b**), P2p (**c**, **d**), O 1 s (**e**, **f**), N 1 s (**g**, **h**) of MIL-101(Cr)-PMIDA before and after adsorption of U (VI)

Acknowledgements The financial support from the Hengyang Science and Technology Plan Project of China (NO. 202002042158) and the Hunan Province Natural Science Foundation of China (NO. 2020JJ4077 and NO. 2020JJ6050) are gratefully acknowledged.

Declarations

Conflict of interest All authors declare no conflict of interest.

References

1. Yang W, Bai ZQ, Shi WQ, Yuan LY, Tian T, Chai ZF, Wang H, Sun ZM (2013) MOF-76: from a luminescent probe to highly efficient U(VI) sorption material. Chem Commun (Camb) 49(88):10415–10417
2. Xiong J, Fan Y, Luo F (2020) Grafting functional groups in metal-organic frameworks for U(VI) sorption from aqueous solutions. Dalton Trans 49(36):12536–12545
3. Yin N, Ai Y, Xu Y, Ouyang Y, Yang P (2020) Preparation of magnetic biomass-carbon aerogel and its application for adsorption of uranium(VI). J Radioanal Nucl Chem 326(2):1307–1321

4. Huang S, Pang H, Li L, Jiang S, Wen T, Zhuang L, Hu B, Wang X (2018) Unexpected ultrafast and high adsorption of U(VI) and Eu(III) from solution using porous Al_2O_3 microspheres derived from MIL-53. Chem Eng J 353:157–166
5. Cheng Y, Sun X, Liao X, Shi B (2011) Adsorptive recovery of uranium from nuclear fuel industrial wastewater by titanium loaded collagen fiber. Chin J Chem Eng 19(4):592–597
6. Acharya R, Parida K (2020) A review on adsorptive remediation of Cr (VI) by magnetic iron oxides and their modified forms. Biointerface Res Appl Chem 10(2):5266–5272
7. Prakash Tripathy S, Acharya R, Das M, Acharya R, Parida K (2020) Adsorptive remediation of Cr (VI) from aqueous solution using cobalt ferrite: Kinetics and isotherm studies. Mater Today: Proceed 30:289–293
8. Acharya R, Naik B, Parida K (2018) Cr(VI) remediation from aqueous environment through modified-TiO2-mediated photocatalytic reduction. Beilstein J Nanotechnol 9:1448–1470
9. Acharya R, Lenka A, Parida K (2021) Magnetite modified amino group based polymer nanocomposites towards efficient adsorptive detoxification of aqueous Cr (VI): A review. J Mol Liq 337:116487
10. Manos MJ, Kanatzidis MG (2012) Layered metal sulfides capture uranium from seawater. J Am Chem Soc 134(39):16441–16446
11. Farjana SH, Huda N, Mahmud MAP, Lang C (2018) Comparative life-cycle assessment of uranium extraction processes. J Clean Prod 202:666–683
12. Zhang N, Xing Y-H, Bai F-Y (2020) Triazine functionalized porous three-dimensional uranyl-organic framework: extraction of uranium(VI) and adsorption of cationic dyes in aqueous solution. Cryst Growth Des 20(3):1838–1848
13. Tavakoli H, Sepehrian H, Semnani F, Samadfam M (2013) Recovery of uranium from UCF liquid waste by anion exchange resin CG-400: breakthrough curves, elution behavior and modeling studies. Ann Nucl Energy 54:149–153
14. Fu F, Xie L, Tang B, Wang Q, Jiang S (2012) Application of a novel strategy-Advanced Fenton-chemical precipitation to the treatment of strong stability chelated heavy metal containing wastewater. Chem Eng J 189–190:283–287
15. Pu Y-q, Xiao F, He S, Wang C, Peng G-w, Liu Y (2017) Synthesis of the p-tert-butyl calix[4] arene symmetrical sulfide derivatives and its extraction properties towards U(VI) from aqueous solution. J Radioanal Nucl Chem 314(3):2137–2143
16. Shuibo X, Chun Z, Xinghuo Z, Jing Y, Xiaojian Z, Jingsong W (2009) Removal of uranium (VI) from aqueous solution by adsorption of hematite. J Environ Radioact 100(2):162–166
17. Xie Y, Chen C, Ren X, Wang X, Wang H, Wang X (2019) Emerging natural and tailored materials for uranium-contaminated water treatment and environmental remediation. Prog Mater Sci 103:180–234
18. Acharya R, Naik B, and Parida KM (2018) Adsorption of Cr (VI) and textile dyes on to mesoporous silica, titanate nanotubes, and layered double hydroxides. Nanomaterials in the Wet Processing of Textiles 219–260
19. Acharya R, Martha S, and Parida KM (2017) Remediation of Cr (VI) using clay minerals, biomasses and industrial wastes as adsorbents. Advanced materials for wastewater treatment 129–170
20. Saleh TA, Naeemullah TM, Sarı A (2017) Polyethylenimine modified activated carbon as novel magnetic adsorbent for the removal of uranium from aqueous solution. Chem Eng Res Des 117:218–227
21. Wang G, Wang X, Chai X, Liu J, Deng N (2010) Adsorption of uranium (VI) from aqueous solution on calcined and acid-activated kaolin. Appl Clay Sci 47(3–4):448–451
22. Samokhvalov A (2018) Aluminum metal–organic frameworks for sorption in solution: A review. Coord Chem Rev 374:236–253
23. Hu R, Shao D, Wang X (2014) Graphene oxide/polypyrrole composites for highly selective enrichment of U(vi) from aqueous solutions. Polym Chem 5(21):6207–6215
24. Viltres H, López YC, Gupta NK, Leyva C, Paz R, Gupta A, Sengupta A (2020) Functional metal-organic frameworks for metal removal from aqueous solutions. Separation & Purification Reviews 1–22
25. Prakash Tripathy S, Subudhi S, Das S, Kumar Ghosh M, Das M, Acharya R, Acharya R, Parida K (2021) Hydrolytically stable citrate capped Fe_3O_4@UiO-66-NH_2 MOF: A hetero-structure composite with enhanced activity towards Cr (VI) adsorption and photocatalytic H2 evolution. J Colloid Interface Sci 606(Pt 1):353–366
26. Yin D, Ren H, Li C, Liu J, Liang C (2018) Highly selective hydrogenation of furfural to tetrahydrofurfuryl alcohol over MIL-101(Cr)-NH_2 supported Pd catalyst at low temperature. Chin J Catal 39(2):319–326
27. Castellanos S, Sai Sankar Gupta KB, Pustovarenko A, Dikhtiarenko A, Nasalevich M, Atienzar P, García H, Gascon J, Kapteijn F (2015) Anchoring of diphenylphosphinyl groups to NH_2-MIL-53 by post-synthetic modification. Eur J Inorg Chem 2015(28):4648–4652
28. Yang D, Gates BC (2019) Catalysis by metal organic frameworks: perspective and suggestions for future research. ACS Catal 9(3):1779–1798
29. Lawson HD, Walton SP, Chan C (2021) Metal-organic frameworks for drug delivery: a design perspective. ACS Appl Mater Interfaces 13(6):7004–7020
30. Tripathi S, Sreenivasulu B, Suresh A, Rao CVSB, Sivaraman N (2020) Assorted functionality-appended UiO-66-NH_2 for highly efficient uranium(vi) sorption at acidic/neutral/basic pH. RSC Adv 10(25):14650–14661
31. Liu J-m, Liu T, Wang C-c, Yin X-h, Xiong Z-h (2017) Introduction of amidoxime groups into metal-organic frameworks to synthesize MIL-53(Al)-AO for enhanced U(VI) sorption. J Mol Liq 242:531–536
32. Liu J-m, Yin X-h, Liu T (2019) Amidoxime-functionalized metal-organic frameworks UiO-66 for U(VI) adsorption from aqueous solution. J Taiwan Inst Chem Eng 95:416–423
33. Wu Y, Pang H, Yao W, Wang X, Yu S, Yu Z, Wang X (2018) Synthesis of rod-like metal-organic framework (MOF-5) nanomaterial for efficient removal of U(VI): batch experiments and spectroscopy study. Science Bulletin 63(13):831–839
34. Ding M, Cai X, Jiang HL (2019) Improving MOF stability: approaches and applications. Chem Sci 10(44):10209–10230
35. Bai Z-Q, Yuan L-Y, Zhu L, Liu Z-R, Chu S-Q, Zheng L-R, Zhang J, Chai Z-F, Shi W-Q (2015) Introduction of amino groups into acid-resistant MOFs for enhanced U(vi) sorption. J Mater Chem A 3(2):525–534
36. Zhang JY, Zhang N, Zhang L, Fang Y, Deng W, Yu M, Wang Z, Li L, Liu X, Li J (2015) Adsorption of uranyl ions on amine-functionalization of MIL-101(Cr) nanoparticles by a facile coordination-based post-synthetic strategy and X-ray absorption spectroscopy studies. Sci Rep 5:13514
37. De Decker J, Folens K, De Clercq J, Meledina M, Van Tendeloo G, Du Laing G, Van Der Voort P (2017) Ship-in-a-bottle CMPO in MIL-101(Cr) for selective uranium recovery from aqueous streams through adsorption. J Hazard Mater 335:1–9
38. Wu H, Chi F, Zhang S, Wen J, Xiong J, Hu S (2019) Control of pore chemistry in metal-organic frameworks for selective uranium extraction from seawater. Microporous Mesoporous Mater 288:109567
39. Mhatre AM, Chappa S, Chaudhari CV, Bhardwaj YK, Pandey AK (2018) Phosphate functionalized radiation grafted Teflon for capturing and quantifications of U(VI) and Pu(IV) ions at

ultra-trace concentration in aqueous samples. J Radioanal Nucl Chem 317(2):1141–1149
40. Nie X, Jiang Y, Dong F, Cheng W, Wang J, Ding C, Liu M, Zhang Y, Xia X (2021) Amide and phosphate groups modified bifunctional luffa fiber for highly efficient removal of U(VI) from real uranium wastewater. J Radioanal Nucl Chem 328(2):591–604
41. Shao D, Li Y, Wang X, Hu S, Wen J, Xiong J, Asiri AM, Marwani HM (2017) Phosphate-Functionalized Polyethylene with High Adsorption of Uranium(VI). ACS Omega 2(7):3267–3275
42. Carboni M, Abney CW, Liu S, Lin W (2013) Highly porous and stable metal–organic frameworks for uranium extraction. Chem Sci 4(6):2396–2402
43. De Decker J, Rochette J, De Clercq J, Florek J, Van Der Voort P (2017) Carbamoylmethylphosphine oxide-functionalized MIL-101(Cr) as highly selective uranium adsorbent. Anal Chem 89(11):5678–5682
44. Li X, Pi Y, Xia Q, Li Z, Xiao J (2016) TiO_2 encapsulated in Salicylaldehyde-NH_2-MIL-101(Cr) for enhanced visible light-driven photodegradation of MB. Appl Catal B 191:192–201
45. Lee YR, Yu K, Ravi S, Ahn WS (2018) Selective adsorption of rare earth elements over functionalized Cr-MIL-101. ACS Appl Mater Interfaces 10(28):23918–23927
46. Bernt S, Guillerm V, Serre C, Stock N (2011) Direct covalent post-synthetic chemical modification of Cr-MIL-101 using nitrating acid. Chem Commun (Camb) 47(10):2838–2840
47. Hwang YK, Hong DY, Chang JS, Jhung SH, Seo YK, Kim J, Vimont A, Daturi M, Serre C, Ferey G (2008) Amine grafting on coordinatively unsaturated metal centers of MOFs: consequences for catalysis and metal encapsulation. Angew Chem Int Ed Engl 47(22):4144–4148
48. Tian N, Jia Q, Su H, Zhi Y, Ma A, Wu J, Shan S (2016) The synthesis of mesostructured NH_2-MIL-101(Cr) and kinetic and thermodynamic study in tetracycline aqueous solutions. J Porous Mater 23(5):1269–1278
49. Wu D, Sun Y, Wang Q (2013) Adsorption of lanthanum (III) from aqueous solution using 2-ethylhexyl phosphonic acid mono-2-ethylhexyl ester-grafted magnetic silica nanocomposites. J Hazard Mater 260:409–419
50. Wang H, Ma L, Cao K, Geng J, Liu J, Song Q, Yang X, Li S (2012) Selective solid-phase extraction of uranium by salicylideneimine-functionalized hydrothermal carbon. J Hazard Mater 229–230:321–330
51. Li X, Mao Y, Leng K, Ye G, Sun Y, Xu W (2017) Synthesis of amino-functionalized MIL-101(Cr) with large surface area. Mater Lett 197:192–195
52. Ma X-H, Yang Z, Yao Z-K, Xu Z-L, Tang CY (2017) A facile preparation of novel positively charged MOF/chitosan nanofiltration membranes. J Membr Sci 525:269–276
53. Ryu S, Fonseka C, Naidu G, Loganathan P, Moon H, Kandasamy J, Vigneswaran S (2021) Recovery of rare earth elements (Lu, Y) by adsorption using functionalized SBA-15 and MIL-101 (Cr). Chemosphere 281:130869
54. Yang F, Xie S, Wang G, Yu CW, Liu H, Liu Y (2020) Investigation of a modified metal-organic framework UiO-66 with nanoscale zero-valent iron for removal of uranium (VI) from aqueous solution. Environ Sci Pollut Res Int 27(16):20246–20258
55. Liu L, Fang Y, Meng Y, Wang X, Ma F, Zhang C, Dong H (2020) Efficient adsorbent for recovering uranium from seawater prepared by grafting amidoxime groups on chloromethylated MIL-101(Cr) via diaminomaleonitrile intermediate. Desalination 478:114300
56. Wang C, Xiao F-z, Pu Y-q, Xu Y-l, Xu D-y, Zhang K, Liu Y, Peng G-w (2018) Preparation of p-carboxyphenyl azo calix[4] arene phosphate derivative and its extraction properties toward uranium(VI). J Radioanal Nucl Chem 317(3):1235–1241
57. Yuan L-Y, Liu Y-L, Shi W-Q, Li Z-j, Lan J-H, Feng Y-X, Zhao Y-L, Yuan Y-L, Chai Z-F (2012) A novel mesoporous material for uranium extraction, dihydroimidazole functionalized SBA-15. J Mater Chem 22(33):17019–17026
58. Duan S, Liu X, Wang Y, Shao D, Alharbi NS, Alsaedi A, Li J (2016) Highly efficient entrapment of U(VI) by using porous magnetic $Ni_{0.6}Fe_{2.4}O_4$ micro-particles as the adsorbent. J Taiwan Inst Chem Eng 65:367–377
59. Budnyak TM, Strizhak AV, Gladysz-Plaska A, Sternik D, Komarov IV, Kolodynska D, Majdan M, Tertykh Vcapital AC (2016) Silica with immobilized phosphinic acid-derivative for uranium extraction. J Hazard Mater 314:326–340
60. Qian Y, Yuan Y, Wang H, Liu H, Zhang J, Shi S, Guo Z, Wang N (2018) Highly efficient uranium adsorption by salicylaldoxime/polydopamine graphene oxide nanocomposites. J Mater Chem A 6(48):24676–24685
61. Liu X, Sun J, Xu X, Alsaedi A, Hayat T, Li J (2019) Adsorption and desorption of U(VI) on different-size graphene oxide. Chem Eng J 360:941–950
62. Xu Y, Zhang K, Wang C, Zhu Q, Luo J, Chen F, Xiao F, Peng G (2020) Fabrication of magnetic functionalized m-carboxyphenyl azo calix[4]arene amine oxime derivatives for highly efficient and selective adsorption of uranium (VI). J Radioanal Nucl Chem 323(3):1145–1155
63. Zhao Y, Li J, Zhao L, Zhang S, Huang Y, Wu X, Wang X (2014) Synthesis of amidoxime-functionalized Fe_3O_4@SiO_2 core–shell magnetic microspheres for highly efficient sorption of U(VI). Chem Eng J 235:275–283
64. Yang P, Liu Q, Liu J, Zhang H, Li Z, Li R, Liu L, Wang J (2017) Interfacial growth of a metal–organic framework (UiO-66) on functionalized graphene oxide (GO) as a suitable seawater adsorbent for extraction of uranium(vi). J Mater Chem A 5(34):17933–17942
65. Perry DL (2015) The tris(carbonato)dioxouranium(VI) ion: A structural model for uranium 4f7/2, 5/2 X-ray photoelectron spectra satellite structures for oxide and oxygen coordination cores. Vacuum 114:162–165
66. Ghanadpour M, Carosio F, Larsson PT, Wagberg L (2015) Phosphorylated cellulose nanofibrils: a renewable nanomaterial for the preparation of intrinsically flame-retardant materials. Biomacromol 16(10):3399–3410
67. Wang L, Dong X, Jiang H, Li G, Zhang M (2014) Phosphorylated ordered mesoporous carbon as a novel solid acid catalyst for the esterification of oleic acid. Catal Commun 56:164–167
68. Ju P, Guo H, Bai J, Liu Q, Zhang H, Liu J, Yu J, Chen R, Wang J (2020) Construction of gel-like swollen-layer on polyacrylonitrile surface and its swelling behavior and uranium adsorption properties. J Colloid Interface Sci 576:109–118
69. Liu X, Li J, Wang X, Chen C, Wang X (2015) High performance of phosphate-functionalized graphene oxide for the selective adsorption of U(VI) from acidic solution. J Nucl Mater 466:56–64
70. Yang D, Wang X, Wang N, Zhao G, Song G, Chen D, Liang Y, Wen T, Wang H, Hayat T, Alsaedi A, Wang X, Wang S (2018) In-situ growth of hierarchical layered double hydroxide on polydopamine-encapsulated hollow Fe_3O_4 microspheres for efficient removal and recovery of U(VI). J Clean Prod 172:2033–2044
71. Husnain SM, Kim HJ, Um W, Chang Y-Y, Chang Y-S (2017) Superparamagnetic adsorbent based on phosphonate grafted mesoporous carbon for uranium removal. Ind Eng Chem Res 56(35):9821–9830